Semiconductor Heterostructures and Low-Dimensional Quantum Structures

15

15.1 Introduction

In Chap. 4, we have introduced the basic concepts and formalism of quantum mechanics. In Chap. 5, we have determined the energy spectrum, or energy-momentum or E–k relations, for electrons in a crystal which governs their interaction with external forces and fields. Moreover, we saw that the quantum behavior of particles is best observed in small, typically nanometer scale (one billionth of a meter or 10^{-9} m) dimension structures, as illustrated in the example of a particle in a 1D box.

In nanometer-scale structures in a crystal, the motion of an electron can be confined in one or more directions in space. When only one dimension is restricted while the other two remain free, we talk about a quantum well; when two dimensions are restricted, we talk about a quantum wire; and when the motion in all three dimensions is confined, we talk about a quantum dot. In solid-state engineering, these are commonly called *low-dimensional quantum structures*.

In the past few decades, progress in semiconductor crystal growth technology, such as liquid-phase epitaxy (LPE), molecular beam epitaxy (MBE), and metal-organic chemical vapor deposition (MOCVD), has made it possible to control with atomic-scale precision of the dimensions of semiconductor structures and thus to realize such low-dimensional quantum structures through the formation of heterojunctions or heterostructures. A semiconductor heterojunction is formed when two different semiconducting materials are brought into direct contact with each other, while heterostructures can be defined as materials that incorporate one or more heterojunctions and can describe more complicated device architectures such as multiple quantum wells, superlattices, and other low-dimensional quantum structures.

First proposed by Shockley in 1951 in a heterojunction bipolar transistor (HBT) (Shockley 1951), heterojunctions have been used heavily in a variety of applications. Many conventional devices take advantage of the special properties of

M. Razeghi, *Fundamentals of Solid State Engineering*,
https://doi.org/10.1007/978-3-319-75708-7_15

heterostructures including semiconductor lasers, light-emitting diodes, photodetectors, etc.

There exist several inherent design advantages to using heterojunctions as opposed to standard homojunctions in semiconductor devices. Due to pairing small- and wide-bandgap materials or by tailoring their lineup energy position, charge carriers can be confined or redistributed. This offers the chance to control, to considerable extent, the physical location of free electrons and holes within the device as well as the wavefunction overlap between the carrier types. Furthermore, by choosing the semiconducting materials and the doping level, important properties of the heterostructure device can be designed. This includes the bandgap, the effective mass, and the carrier transport. Finally, depending on the lattice mismatch between the heterojunction materials, built-in strain fields can be engineered and used to obtain enhanced electrical or optical properties.

This chapter will first review the concepts associated with semiconductor heterostructures, including energy band offsets, types of alignment, and a few models for heterojunction energy band alignment. Then, the properties of low-dimensional quantum structures will be discussed in detail.

15.2 Energy Band Offsets

When a heterojunction is formed, the conduction and valence band alignment is dependent upon the properties of the constituent materials such as their bandgap, the doping, and the electron affinity. Heterostructures can be classified depending on the band alignment formation between the two semiconductor materials. The possible band alignment combinations include “type I,” “type II staggered,” and “type II broken gap” and are described below.

15.2.1 Type I Alignment

When the valence and conduction band of one material “straddles” the bands of the narrow-gap material, the heterojunction band alignment is termed type I. The heavily investigated AlGaAs/GaAs heterojunction exhibits this band lineup with the aluminum-containing material having its conduction band above and valence band below the corresponding GaAs band energies. An example of type I band alignment is shown in Fig. 15.1a. The schematic figure shows materials in electrical isolation from one another. As we will see later in this chapter, direct interaction between semiconductor materials results in space-charge redistribution, which leads to band bending near the junction position.

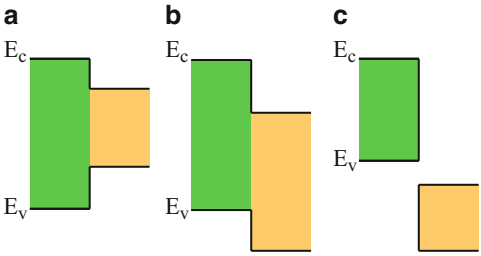

Fig. 15.1 Heterojunction band lineups for isolated but adjacent semiconductors: (**a**) type I, (**b**) type II staggered, and (**c**) type II broken gap alignments

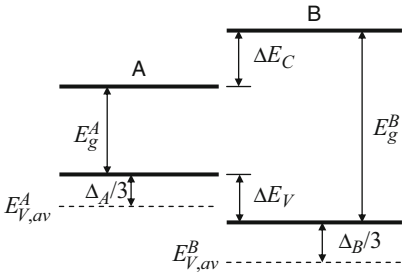

Fig. 15.2 Band alignment diagram for calculation of band offset

15.2.2 Type II Alignments

Semiconductor heterojunctions may also form where the conduction and valence bands in one material are both slightly below the corresponding band energies in the adjacent semiconductor. This band alignment is termed type II staggered and is shown in Fig. 15.1b. One example of a heterojunction material system that can be generally classified as type II staggered is InAs/AlSb.

The InAs/GaSb heterojunction is an example of a type II broken gap alignment. This occurs when the conduction of one material is at a lower energy than the valence band of the adjacent semiconductor. An example of broken-gap band alignment is shown in Fig. 15.1c.

15.3 Application of Model Solid Theory

In the previous sections, we have introduced different types of band lineups. In order to better understand the heterojunction properties, it is important to determine the actual band lineups between two different materials. We introduce the application of model solid theory for this type of calculation. For simplicity, we consider unstrained junctions only. This is true for the GaAs/$Al_xGa_{1-x}As$ ($0 < x < 0.4$) junction system.

We assume A and B in Fig. 15.2 represent two III–V semiconductors that have the same lattice constant. The valence band position can be calculated as:

$$E_V = E_{V,av} + \frac{\Delta}{3} \tag{15.1}$$

in which $E_{V,av}$ is the average valence band position which is obtained from theory and is referred to as the absolute energy level, E_V is the valence band position, and Δ is the spin-orbit splitting energy. The values for different semiconductors are usually tabulated in the literature.

The valence band offset between semiconductor A and B thus can be calculated as:

$$\Delta E_V = \left(E_{V,av}^A - E_{V,av}^B\right) + \frac{1}{3}(\Delta_A - \Delta_B) \tag{15.2}$$

The conduction band edge is obtained by adding the bandgap value to the valence band position:

$$E_C = E_V + E_g \tag{15.3}$$

Therefore the conduction band offset can be calculated as:

$$\Delta E_C = \left(E_{V,av}^A - E_{V,av}^B\right) + \frac{1}{3}(\Delta_A - \Delta_B) + \left(E_g^A - E_g^B\right) \tag{15.4}$$

All these quantities are summarized in Fig. 15.2.

Example
Q: Determine the band offset of a GaAs/$Al_{0.2}Ga_{0.8}As$ heterojunction. The material parameters for GaAs and AlAs are listed in Table 15.1.
A: For GaAs, we have:

$$E_V^{GaAs} = E_{V,av}^{GaAs} + \frac{\Delta_{GaAs}}{3} = -6.807\text{eV}$$

For $Al_{0.2}Ga_{0.8}As$, we use the arithmetic average of 20% AlAs and 80% of GaAs:

$$\begin{aligned} E_V^{Al_{0.2}Ga_{0.8}As} &= 0.2 \times \left(E_{V,av}^{AlAs} + \frac{\Delta_{AlAs}}{3}\right) + 0.8 \times \left(E_{V,av}^{GaAs} + \frac{\Delta_{GaAs}}{3}\right) \\ &= -6.925\text{eV} \end{aligned}$$

$$E_g^{Al_{0.2}Ga_{0.8}As} = 0.2 \times E_g^{AlAs} + 0.8 \times E_g^{GaAs} = 1.842\text{eV}$$

Table 15.1 Material parameters for GaAs and AlAs

	$E_{V,av}$ (eV)	Δ(eV)	E_g(eV)
GaAs	−6.92	0.34	1.52
AlAs	−7.49	0.28	3.13

Therefore, we obtain the band offset as follows:

$$\begin{cases} \Delta E_{\mathrm{V}} = E_{\mathrm{V}}^{\mathrm{GaAs}} - E_{\mathrm{V}}^{\mathrm{Al_{0.2}Ga_{0.8}As}} = (-6.807) - (-6.925) \\ \qquad = 0.118\mathrm{eV} \\ \Delta E_{\mathrm{C}} = \left(E_{\mathrm{V}}^{\mathrm{Al_{0.2}Ga_{0.8}As}} + E_{\mathrm{g}}^{\mathrm{Al_{0.2}Ga_{0.8}As}}\right) - \left(E_{\mathrm{V}}^{\mathrm{GaAs}} + E_{\mathrm{g}}^{\mathrm{GaAs}}\right) \\ \qquad = (-5.287) - (-5.555) \\ \qquad = 0.268\mathrm{eV} \end{cases}$$

15.4 Anderson Model for Heterojunctions

When we bring two different semiconductors in contact with each other, due to their difference of the Fermi level with respect to the vacuum level, there will be net charge transfer from one material to the other. At equilibrium, the Fermi level lines up on both sides of the junction. This will change the band diagram of the heterojunction from straight lines to partially rounded curves. In this section, we use the basic Anderson model to calculate the zero-bias band diagram for a *p-n* junction made from a type I heterojunction, with N_{A} representing the *p*-type doping level of the narrower-gap material and N_{D} the *n*-type doping level of the wider-gap material. The other cases of *p-n* heterojunctions can be derived in a same manner and will not be covered.

To simplify the calculations and emphasize the methodology that will be introduced, we assume that both N_{A} and N_{D} are much larger than the intrinsic carrier concentration and that all the dopants are ionized. Before contact, the Fermi level on each side is represented as $E_{\mathrm{F_A}}$ and $E_{\mathrm{F_B}}$. We use V_0 to represent the potential difference due to the energy difference between $E_{\mathrm{F_A}}$ and $E_{\mathrm{F_B}}$, as shown in Fig. 15.2. According to Fig. 15.2, we have:

$$V_0 = E_{\mathrm{g}}^{\mathrm{A}} + \Delta E_{\mathrm{C}} - \left(E_{\mathrm{F_A}} - E_{\mathrm{V}}^{\mathrm{A}}\right) - \left(E_{\mathrm{C}}^{\mathrm{B}} - E_{\mathrm{F_B}}\right) \tag{15.5}$$

For nondegenerate semiconductors, we have:

$$\begin{cases} E_{\mathrm{F_A}} - E_{\mathrm{V}}^{\mathrm{A}} = -k_{\mathrm{b}} T \ln\left(\dfrac{N_{\mathrm{A}}}{N_{\mathrm{v}}^{\mathrm{A}}}\right) \\ E_{\mathrm{V}}^{\mathrm{B}} - E_{\mathrm{F_B}} = -k_{\mathrm{b}} T \ln\left(\dfrac{N_{\mathrm{d}}}{N_{\mathrm{c}}^{\mathrm{B}}}\right) \end{cases} \tag{15.6}$$

where $N_{\mathrm{v}}^{\mathrm{A}}$ and $N_{\mathrm{c}}^{\mathrm{B}}$ are the valence band and conduction-band density of states for semiconductor A and B, respectively. Substituting Eq. (15.6) into Eq. (15.5), we obtain the expression for V_0:

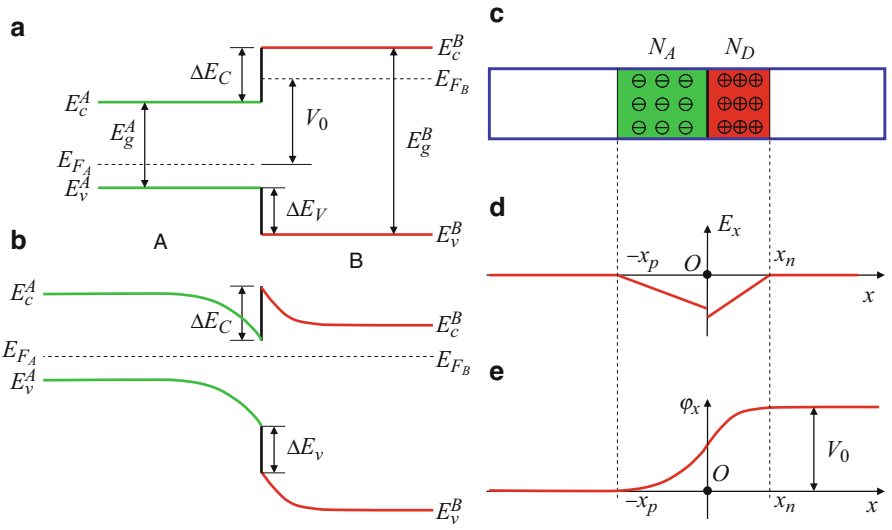

Fig. 15.3 Illustrations for (**a**) band diagram for the heterojunction before charge transfer, (**b**) band diagram after charge transfer, (**c**) depletion approximation, (**d**) electric field distribution, and (**e**) electrical potential distribution

$$V_0 = E_{\mathrm{g}}^{\mathrm{A}} + \Delta E_{\mathrm{C}} + k_{\mathrm{b}} T \ln\left(\frac{N_{\mathrm{A}} \cdot N_{\mathrm{D}}}{N_{\mathrm{v}}^{\mathrm{A}} \cdot N_{\mathrm{c}}^{\mathrm{B}}}\right) \tag{15.7}$$

After we bring semiconductor A and B together into contact, there will be a net electron transfer from B to A (see Fig. 15.3c) until the Fermi levels on both sides reach the same value, as shown in Fig. 15.3b.

The number of excess negative charges (ionized acceptors) on the *p*-side will be exactly the same as that of the excess positive charges (ionized donors) on the n-side. N_{a} and N_{d} equal the charge densities on the p and n-sides of the junction within the depletion region. Thus we have the charge conservation equation:

$$N_{\mathrm{A}} x_p = N_{\mathrm{D}} x_n \tag{15.8}$$

We assume that the charge density is uniformly distributed on either side of the junction over a certain distance. This is called the depletion approximation. Under this approximation, we can calculate the electric field distribution and thus the electrical potential profile.

Assume that ε_{A} and ε_{B} represent the relative permittivity for semiconductor A and B. Using Gauss' law, we can obtain the electric field within the depletion region as:

$$\begin{cases} E_x = -\dfrac{qN_{\mathrm{A}}(x + x_p)}{\varepsilon_{\mathrm{A}}\varepsilon_0}, & -x_p \le x < 0 \\ E_x = -\dfrac{qN_{\mathrm{D}}(x_n - x)}{\varepsilon_{\mathrm{B}}\varepsilon_0}, & 0 < x \le x_n \end{cases} \tag{15.9}$$

Outside the depletion region, the net charge density is zero, and there is no electric field. We take the zero potential to be at the neutral region in the semiconductor A. We integrate the electric field from the point of calculation toward the potential zero point to obtain the electrical potential profile:

$$\varphi_x = \int_x^{-x_p} E_x dx \tag{15.10}$$

Substituting Eq. (15.9) into Eq. (15.10), we have:

$$\begin{cases} \varphi_x = 0, & x < -x_p \\ \varphi_x = \dfrac{qN_{\mathrm{A}}\left(x + x_p\right)^2}{2\varepsilon_{\mathrm{A}}\varepsilon_0}, & -x_p \le x < 0 \\ \varphi_x = \dfrac{qN_{\mathrm{A}}x_p^2}{2\varepsilon_{\mathrm{A}}\varepsilon_0} + \dfrac{qN_{\mathrm{D}}(2x_n x - x^2)}{2\varepsilon_{\mathrm{B}}\varepsilon_0}, & 0 \le x \le x_n \\ \varphi_x = \dfrac{qN_{\mathrm{A}}x_p^2}{2\varepsilon_{\mathrm{A}}\varepsilon_0} + \dfrac{qN_{\mathrm{D}}x_n^2}{2\varepsilon_{\mathrm{B}}\varepsilon_0}, & x > x_n \end{cases} \tag{15.11}$$

We recall that the total potential drop is V_0 as calculated before, i.e.,

$$\frac{qN_{\mathrm{A}}x_p^2}{2\varepsilon_{\mathrm{A}}\varepsilon_0} + \frac{qN_{\mathrm{D}}x_n^2}{2\varepsilon_{\mathrm{B}}\varepsilon_0} = V_0 \tag{15.12}$$

Combining Eq. (15.8) and Eq. (15.12), we obtain the values of x_{n} and x_{p} in terms of V_0:

$$\begin{cases} x_n = \sqrt{\dfrac{N_{\mathrm{A}}}{N_{\mathrm{D}}} \dfrac{2\varepsilon_0 V_0}{q} \dfrac{\varepsilon_{\mathrm{A}}\varepsilon_{\mathrm{B}}}{N_{\mathrm{A}}\varepsilon_A + N_{\mathrm{D}}\varepsilon_{\mathrm{B}}}} \\ x_p = \sqrt{\dfrac{N_{\mathrm{D}}}{N_{\mathrm{A}}} \dfrac{2\varepsilon_0 V_0}{q} \dfrac{\varepsilon_{\mathrm{A}}\varepsilon_{\mathrm{B}}}{N_{\mathrm{A}}\varepsilon_{\mathrm{A}} + N_{\mathrm{D}}\varepsilon_{\mathrm{B}}}} \end{cases} \tag{15.13}$$

We define the junction depletion width as $x_{\mathrm{w}} = x_{\mathrm{n}} + x_{\mathrm{p}}$. Taking into account Eq. (15.13), we can obtain:

$$x_w = \sqrt{\frac{2\varepsilon_0 V_0}{qN_{\mathrm{D}}N_{\mathrm{A}}} \frac{\varepsilon_{\mathrm{A}}\varepsilon_{\mathrm{B}}}{N_{\mathrm{A}}\varepsilon_{\mathrm{A}} + N_{\mathrm{D}}\varepsilon_{\mathrm{B}}}} \cdot (N_{\mathrm{D}} + N_{\mathrm{A}}) \tag{15.14}$$

Substituting Eq. (15.13) into Eq. (15.12), we will obtain the values for the electrical potential φ_x. In order to update the electron energy band diagram, we need to take into account that the electron charge is negative and the electron energy profile will be inverted. Adding this energy profile to the flat band profile as shown in Fig. 15.3a, we will obtain a calculated electron energy profile for the heterojunction under equilibrium as illustrated in Fig. 15.3b.

15.5 Multiple Quantum Wells and Superlattices

By "sandwiching" a low-bandgap material between two layers of wider bandgap material, a device designer can fabricate a single quantum well, as discussed later in this chapter. A layer of GaAs between two $Al_xGa_{1-x}As$ barriers acts as a potential well for electrons and holes. By adjusting the well width and composition of the barriers, one can engineer specific properties into the quantum well structure such as the energy bandgap.

In a similar fashion, multiple quantum wells (MQWs) may be formed by epitaxy of successive, periodic heterojunctions. Typically within MQWs, the carriers within a quantum well do not interact with carriers in a neighboring well. In other words, the electron and hole wavefunctions between adjacent wells do not overlap. Depending on the band alignment type of the heterojunctions involved, electrons and holes can be confined in similar or different spatial locations in the multiple quantum well structure. Multiple quantum wells are used in devices like quantum well intersubband photodetectors (QWIP) for enhanced absorption over a thicker active region.

Superlattices are structures that also have periodic heterojunctions similar to multiple quantum wells. However, the confined charge carriers within the individual quantum wells actively interact with carriers in other wells. This can be achieved by decreasing the quantum well barrier thickness in a multiple quantum well structure. The electron is now delocalized and can move from well to well just as in a Kronig-Penney lattice. Over an extended length span (many superlattice periods), electrons in superlattices can therefore exhibit miniband behavior, similar to bulk crystals. By controlling the layer structure, the superlattice band structure can be engineered. One can enhance desired effects such as optical emission/absorption or reduce unwanted effects such as Auger recombination. In addition, properties such as tunneling transport can be modified. An example of an epitaxially grown InAs/GaSb superlattice is shown in Fig. 15.4.

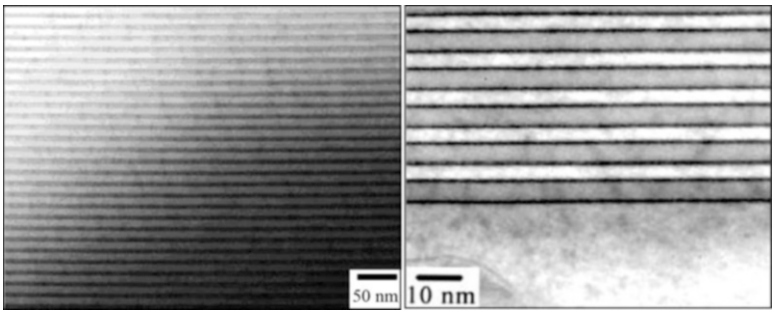

Fig. 15.4 Transmission electron microscope images of type II InAs/GaSb superlattice. The dark regions correspond to the InSb interface between InAs and GaSb layers (by courtesy of G Brown)

15.6 Two-Dimensional Structures: Quantum Wells

15.6.1 Energy Spectrum

As briefly mentioned previously, a quantum well is formed when the motion of electrons is confined in one direction (e.g., x), while it remains free to move in the other two directions (y, z). This situation is most easily achieved by sandwiching a thin and flat film semiconductor crystal between two crystals of another other semiconductor material in such a way that a potential step is produced, as shown in Fig. 15.5. The electrons are confined in the region $0 < x < a$. In the following discussion, we chose U_0, the potential step, to be finite.

This energy profile is in fact a potential that an electron experiences when moving through the structure. This is in addition to the crystal periodic potential of Chap. 3, which will not be brought into the discussion as it is already taken into account by considering an effective mass for the electron.

The potential in the x-direction is analogous to the case of a particle in a finite potential well as discussed in Sect. 4.4.4. The height of the potential barrier is now the difference between the conduction band energies in the different semiconductors, which is called the conduction band offset and denoted ΔE_c. The contribution to potential in the y- and z-directions is constant and is chosen to be zero, similar to the case of a free particle, as discussed in Sect. 4.4.1. The total potential can therefore be expressed as:

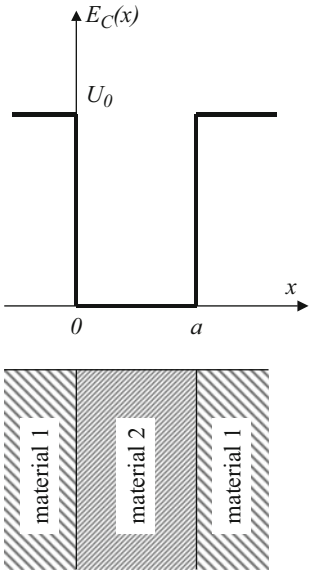

Fig. 15.5 Potential energy profile of a quantum well. This profile can be obtained by sandwiching a thin and flat semiconductor film of material 2 between two semiconductor crystals of another material 1

$$U(x,y,z) = \begin{cases} 0 & \text{for } 0 < x < a \\ U_0 > 0 & \text{for } x < 0 \text{ and } x > a \end{cases}, \tag{15.15}$$

and the time-independent Schrödinger equation becomes:

$$-\frac{\hbar^2}{2m^*}\nabla^2\Psi(x,y,z) - [E - U(x,y,z)]\Psi(x,y,z) = 0 \tag{15.16}$$

where m^* is the electron effective mass. The shape of the potential in Eq. (15.15) implies that the motion in the x-direction and that in the (y,z)-plane are independent. It is a common practice to use the subscripts "$\perp$" and "//" to denote the motion and energies for the x-direction and (y,z)-plane, respectively. For example, $\vec{r}$ is used to denote the position vector in the x-direction and $\vec{r}_{//}$ the position vector in the (y,z)-plane. The total three-dimensional wavefunction can therefore be represented by the product of two functions, one dependent on x alone and the other on (y,z) only, $\Psi_{\text{total}}(x,y,z) = \Psi_{//}(\vec{r}_{//})\Psi_{\perp}(\vec{r}_{\perp})$, and the total energy spectrum consists of the sum of two independent contributions: $E(\vec{r}) = E_{//}(\vec{k}_{//}) + E_{\perp}(\vec{k}_{\perp})$. Now let us consider the wavefunctions and energy spectrum in more detail.

In-Plane Motion

In the (y,z)-plane, the motion of the electron is similar to that of a free particle discussed in Sect. 4.4.1. The wavefunction $\Psi_{//}(\vec{r}_{//})$ can therefore be considered to be a plane wave similar to Eq. (4.32) and can be expressed as:

$$\Psi_{//}(\vec{r}_{//}) = A\exp(i\vec{k}_{//}\cdot\vec{r}_{//}) \tag{15.17}$$

where A is a normalization constant. The energy spectrum in the (y,z) plane is given by:

$$E_{//}(\vec{k}_{//}) = \frac{\hbar^2\vec{k}_{//}^{\,2}}{2m^*} = \frac{\hbar^2\left(k_y^2 + k_z^2\right)}{2m^*} \tag{15.18}$$

Note that these expressions are correct only for small values of the momentum such that $\left|\vec{k}_{//}\right| \ll \left|\vec{K}\right|$, where $\vec{K}$ is a reciprocal lattice vector. This restriction arises from the fact that we are not considering a completely free particle but rather an electron in a crystal. For a more precise discussion on what happens near a reciprocal lattice vector, the reader may be referred to the Kronig-Penney model in Chap. 5.

Motion Perpendicular to Well Plane

In the x-direction, the discussion is the same as that of a particle in a finite potential well conducted in Sect. 4.4.4. Although no analytical solution was derived, the main results can be summarized as follows.

The set of equations from Eq. (4.57) to Eq. (4.59) yields the quantized allowed energy levels $E_{\perp n}$, momenta $k_{\perp n}$, and decay coefficients α_n for an electron in this potential well, indexed by an integer $n = 0,1,\ldots$, and these quantities must satisfy Eq. (4.50):

$$\begin{cases} E_{\perp n} = \dfrac{\hbar^2 (k_{\perp n})^2}{2m^*} \\ \alpha_n = \sqrt{\dfrac{2m^*(U_0 - E_{\perp n})}{\hbar^2}} \end{cases} \tag{15.19}$$

Note that we are now using the effective mass of the electron, m^*. The spacing between consecutive energy levels is on the order of $\hbar^2\pi^2/m^*a^2$ from Eq. (4.43). For $E_n < U_0$, the wavefunction $\Psi_\perp\left(\vec{r}_\perp\right) = \Psi_\perp(x)$ consists of an oscillatory function inside the well ($0 < x < a$) and a decaying exponential outside the well. If needed, this wavefunction can be calculated using Eq. (4.51), Eq. (4.53), and the values of $E_{\perp n}$, $k_{\perp n}$, and α_n as illustrated in Fig. 15.6.

For an electron in a perfect crystal, the quantization of the energy levels and momenta is significant only when the dimensions of the confining structure (e.g., a) become on the order of or less than the electron de Broglie wavelength (Eq. (4.1)).

In a real crystal, however, there are defects which introduce perturbations of the potential periodicity. This results in the broadening of the initially discrete energy levels, and the magnitude of this broadening can be estimated to be $\hbar/\tau$ where τ is a characteristic time between electron collisions, or electron lifetime, which can be

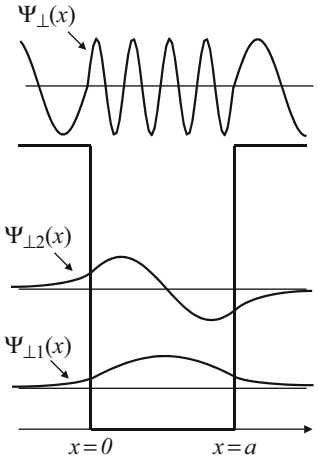

Fig. 15.6 Shapes of the wavefunctions $\Psi_\perp(x)$ for the allowed energy levels of a quantum well. In this example, there are only two allowed confined states. The wavefunctions of these have an oscillatory behavior inside the well ($0 < x < a$) but vanish rapidly when outside the quantum well. A third allowed state is shown which has an energy above the barrier of the well and therefore corresponds to a non-confined state. Its wavefunction has an oscillatory behavior in the entire space

understood as the average duration between two consecutive encounters with defects. A detailed discussion on electron collisions is beyond the scope of this textbook, and the reader is referred to the Further Reading section.

In such a situation, the quantization of the energy levels can be resolved only if the energy spacing between consecutive levels ($\hbar^2\pi^2/m^*a^2$) is larger than the broadening ($\hbar/\tau$). In other words, the inequality $\hbar^2\pi^2/m^*a^2 \gg \hbar/\tau$ ensures that the quantized behavior can be observed.

15.6.2 Density of States

The total energy spectrum for an electron in a quantum well is given by considering Eq. (15.18) and Eq. (15.19):

$$E\left(\vec{k}_{//}, n\right) = E_{//}\left(\vec{k}_{//}\right) + E_{\perp n} = \frac{\hbar^2\,\vec{k}_{//}^{\,2}}{2m^*} + \frac{\hbar^2(k_{\perp n})^2}{2m^*} \tag{15.20}$$

where the values of $\vec{k}_{//}$ are continuous while $k_{\perp n}$ is quantized and indexed by an integer n. Similar to Eq. (5.41) in Sect. 5.3.2, the density of states for quasi-two-dimensional electrons in quantum well is the number of allowed electron energy states (taking into account spin degeneracy) per unit energy interval around an energy E and is given by:

$$g_{2\mathrm{D}}(E) = 2\sum_{n,\,\vec{k}_{//}} \delta\left[E_{//}\left(\vec{k}_{//}\right) + E_{\perp n} - E\right] \tag{15.21}$$

where the factor 2 arises from the spin degeneracy. In this case, because one dimension is quantized while the other two remain continuous, the summation in Eq. (5.44) is performed on two coordinates only:

$$\sum_{\vec{k}_{//}} Y\left(\vec{k}_{//}\right) = \frac{S}{(2\pi)^2}\int\int Y\left(\vec{k}_{//}\right)d\vec{k}_{//} = \frac{S}{(2\pi)^2}\int_{-\infty}^{\infty}\int_{-\infty}^{\infty} Y\left(k_y, k_z\right)dk_y dk_z \tag{15.22}$$

where S is the cross-sectional area of the crystal, in the (y,z)-plane, and $Y\left(\vec{k}_{//}\right)$ is an arbitrary function. Equation (15.21) then becomes:

$$g_{2\mathrm{D}}(E) = \frac{2S}{(2\pi)^2}\sum_{n}\iint_{\vec{k}_{//}} \delta\left[E_{//}\left(\vec{k}_{//}\right) + E_{\perp n} - E\right]d\vec{k}_{//} \tag{15.23}$$

Now, we must determine the relation between $d\left[E_{//}\left(\vec{k}_{//}\right)\right]$ as a function of $d\,\vec{k}_{//}$ in order to perform the integration in Eq. (15.23). For this, we follow the same analysis conducted in Eq. (5.35) to Eq. (5.39). Equation (15.23) yields:

$$d\left[E_{//}\left(\vec{k}_{//}\right)\right] = \frac{\hbar^2}{2m^*}.(2k_{//})dk_{//} \tag{15.24}$$

where $k_{//}$ is the norm or length of the vector $\vec{k}_{//}$. On the other hand, in two dimensions, Eq. (5.37) becomes:

$$d\vec{k}_{//} = d\left(\pi k_{//}^2\right) = 2\pi k_{//}dk_{//} \tag{15.25}$$

Thus:

$$d\left[E_{//}\left(\vec{k}_{//}\right)\right] = \frac{\hbar^2}{2m^*}\frac{1}{\pi}d\vec{k}_{//}, \tag{15.26}$$

and Eq. (15.23) becomes:

$$\begin{cases} g_{2D}(E) = \dfrac{S}{2\pi^2}\left(\dfrac{2m^*\pi}{\hbar^2}\right)\displaystyle\sum_n \int_0^\infty \delta\left[E_{//}\left(\vec{k}_{//}\right) + E_{\perp n} - E\right] d\left[E_{//}\left(\vec{k}_{//}\right)\right] \\ g_{2D}(E) = \dfrac{Sm^*}{\pi\hbar^2}\displaystyle\sum_n \int_0^\infty \delta[x + E_{\perp n} - E]dx \end{cases} \tag{15.27}$$

The integral will be zero if the argument of the Dirac function, i.e., $[x + E_{\perp n} - E]$, never reaches zero when the variable x is varied from 0 to $+\infty$. In other words:

$$\begin{cases} \displaystyle\int_0^\infty \delta[x + E_{\perp n} - E]dx = 0 \quad \text{if} \quad [E_{\perp n} - E] > 0 \\ \displaystyle\int_0^\infty \delta[x + E_{\perp n} - E]dx = 1 \quad \text{if} \quad [E_{\perp n} - E] < 0 \end{cases} \tag{15.28}$$

This can be best expressed by considering the step function which is defined as:

$$\begin{cases} \Theta(X) = 0 \quad \text{for} \quad x < 0 \\ \Theta(X) = 1 \quad \text{for} \quad x > 0 \end{cases} \tag{15.29}$$

Therefore, we can write:

$$\int_0^\infty \delta[x + E_{\perp n} - E]dx = \Theta[E - E_{\perp n}], \tag{15.30}$$

and Eq. (15.27) becomes:

$$g_{2D}(E) = \frac{Sm^*}{\pi\hbar^2} \sum_n \Theta[E - E_{\perp n}] \tag{15.31}$$

This relation expresses that, in a quantum well, the density of states of quasi-two-dimensional electrons is a discontinuous function of energy and is incremented by an amount of $Sm^*/\pi\hbar^2$ each time the energy E crosses an allowed value of $E_{\perp n}$, as shown in Fig. 15.7. At each consecutive value of $E_{\perp n}$, a new two-dimensional energy subband begins. The density of states of each new subband is constant so that we obtain the staircase structure shown in Fig. 15.7.

The modification of the density of states in a quantum well (2D) from that in the bulk case (3D), shown in Fig. 15.7, reflects the change in the motion of an electron. The in-plane motion is two-dimensional, which makes the density of states independent on the energy in a subband. For the motion perpendicular to the well plane, we have a new quantum number n, introduced in Eq. (15.19), which replaces one direction of $\vec{k}$ of the three-dimensional case. The excitation of an electron in this direction results in an increase of the quantum number n and thus a transition to the next subband as illustrated by the staircase in Fig. 15.7.

It can be mathematically demonstrated that the density of states for two-dimensional and three-dimensional electrons does coincide at values of $E = E_{\perp n}$, as illustrated in Fig. 15.7, although this is beyond the scope of this discussion.

This considerable dependence of the density of states on the dimensionality of the structure is a key property of low-dimensional structures which opens new possibilities in device applications.

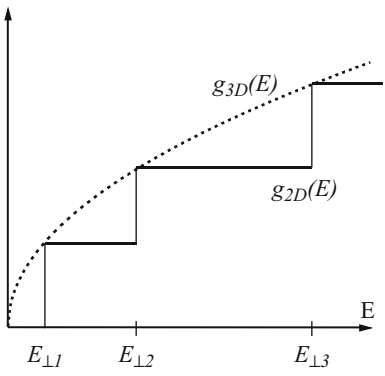

Fig. 15.7 Density of states in the conduction band in a quantum well (2D). The density of states is constant for values of energy between two consecutive quantized energy levels. For comparison, the density of states of a bulk material (3D) is shown in dashed lines

Example
Q: Calculate the number of states between the first and the second energy levels in a quantum well of thickness 25 Å and area of 1 mm^2. Assume that the energy difference between the first two energy levels is 0.3 eV and that the electron effective mass in the quantum well is $m^* = 0.067m_0$ where m_0 is the free electron rest mass.
A: Similar to the three-dimensional case, the number of states is equal to: $N = \int_{E_1}^{E_2} g_{2D}(E)dE$, where E_1 and E_2 are the first and second energy levels in the quantum well, respectively. Since the expression for $g_{2D}(E)$ is given by (we assume $\vec{k}_{//} = \vec{0}$):
$g_{2D}(E) = \frac{Sm^*}{\pi\hbar^2} \sum_n \Theta[E - E_{\perp_n}]$, we obtain:

$$\begin{aligned} N &= \int_{E_1}^{E_2} g_{2D}(E)dE = \frac{Sm^*}{\pi\hbar^2} \sum_n \Theta[E - E_{\perp n}] \\ &= \frac{Sm^*}{\pi\hbar^2}(E_2 - E_1) \\ &= \frac{\left(10^{-3}\right)^2 \left(0.067^* 0.91095 \times 10^{-30}\right)}{\pi\left(1.05458 \times 10^{-34}\right)^2} \left(0.3 \times 1.60218 \times 10^{-19}\right) \\ &\approx 8.40 \times 10^{10} \end{aligned}$$

15.6.3 The Influence of an Effective Mass

In the previous discussion, we have only considered one value for the electron mass m^* for the sake of simplicity. In reality, two effective masses must be considered for the electron in each of the crystals depicted in Fig. 15.5. The effective mass of the electron traveling across the structure thus depends on position, $m^*(x)$. Two Schrödinger equations must then be considered:

$$\begin{cases} -\dfrac{\hbar^2}{2m_1{}^*}\nabla^2\Psi(x,y,z) - [E - U(x,y,z)]\Psi(x,y,z) = 0 \\ \qquad \text{for } x < 0 \text{ and } x > a \\ -\dfrac{\hbar^2}{2m_2{}^*}\nabla^2\Psi(x,y,z) - [E - U(x,y,z)]\Psi(x,y,z) = 0 \\ \qquad \text{for } 0 < x < a \end{cases} \tag{15.32}$$

The other important change concerns the boundary conditions outlined in Eq. (4.52). The continuity of the first derivative of the wavefunction $\partial\Psi(x,y,z)/\partial x$ is no longer valid but must be replaced by the continuity of the product $(1/m^*(x))(\partial\Psi(x,y,z)/\partial x)$, which takes into account the spatial dependence of the electron effective mass. As a result, the boundary conditions in Eq. (4.52) must be replaced by:

$$\begin{cases} \dfrac{1}{m_1^*}\dfrac{\partial \Psi_-}{\partial x}(0) = \dfrac{1}{m_2^*}\dfrac{\partial \Psi_0}{\partial x}(0) \\ \text{and} \\ \dfrac{1}{m_2^*}\dfrac{\partial \Psi_0}{\partial x}(a) = \dfrac{1}{m_1^*}\dfrac{\partial \Psi_+}{\partial x}(a) \end{cases} \tag{15.33}$$

15.7 One-Dimensional Structures: Quantum Wires

15.7.1 Density of States

A quantum wire is formed when the motion of electrons in the conduction band is confined in two directions (e.g., x and y), while it remains free to move in the remaining direction (z). This can be physically achieved by surrounding a small cross-section, rectangular semiconductor crystal with two crystals which have higher bandgap energies.

One way to mathematically treat this situation is to start from the results of a quantum well where the confinement in the x-direction has already been considered and to introduce the confinement in one of the remaining directions (e.g., y). This is not the only way to model quantum wires, and it does not lead to generalized expressions of wavefunctions and energies, but it gives an idea of what is happening. The results can be readily transposed from those of a quantum well and are as follows.

The total wavefunction can be considered as the product of three components:

$$\Psi_{\text{total}}(x, y, z) = \Psi_z(z)\Psi_y(y)\Psi_x(x) \tag{15.34}$$

Only the wavefunction in the z-direction can be easily expressed as a plane wave:

$$\Psi_z(z) = A\exp(ik_z.z) \tag{15.35}$$

where A is a normalization constant. The total energy is the sum of three components:

$$\begin{aligned} E(k_z, n, m) &= E_z(k_z) + (E_x)_n + \left(E_y\right)_m \\ &= \frac{\hbar^2 k_z^2}{2m^*} + \frac{\hbar^2 (k_x)_n^2}{2m^*} + \frac{\hbar^2 \left(k_y\right)_m^2}{2m^*} \end{aligned} \tag{15.36}$$

where n and m are integers (1,2,. . .) used to index the quantized energy levels, $(E_x)_n$ and $(E_y)_m$, and quantized wavenumbers, $(k_x)_n$ and $(k_y)_m$, which result from the confinement of the electron motion in the x- and y-directions, respectively. The values for $(E_x)_n$ and $(E_y)_m$ can be determined, for example, by solving the finite potential well problem in Sect. 4.4.4.

The most important characteristic of a quantum wire is its electron density of states in the conduction band which is given by:

$$g_{1D}(E) = 2\sum_{n,m,k_z} \delta\left[E_z(k_z) + (E_x)_n + \left(E_y\right)_m - E\right] \tag{15.37}$$

In this one-dimensional case, we can make use of the quasi-continuous nature of k_z to write the identity for an arbitrary function $Y(k_z)$:

$$\sum_{k_z} \mathrm{Y}(k_z) \equiv \frac{L}{2\pi}\int_{-\infty}^{+\infty} \mathrm{Y}(k_z)dk_z \tag{15.38}$$

which allows us to simplify Eq. (15.) into:

$$g_{1D}(E) = \frac{2L}{2\pi}\sum_{n,m}\int_{-\infty}^{+\infty} \delta\left[E_z(k_z) + (E_x)_n + \left(E_y\right)_m - E\right]dk_z \tag{15.39}$$

where L is the length of the quantum wire. Moreover, in the one-dimensional case, we have:

$$d[E_z(k_z)] = \frac{\hbar^2}{m^*}k_z dk_z = \frac{\hbar^2}{m^*}\sqrt{\frac{2m^* E_z(k_z)}{\hbar^2}}dk_z \tag{15.40}$$

Therefore, Eq. (15.39) becomes:

$$\begin{cases} g_{1D}(E) = \dfrac{L}{\pi}\sqrt{\dfrac{m^*}{2\hbar^2}}\displaystyle\sum_{n,m}\int_0^{+\infty} \delta\left[E_z(k_z) + (E_x)_n + \left(E_y\right)_m - E\right]\frac{1}{\sqrt{E_z(k_z)}}dE_z \\ \text{or} \\ g_{1D}(E) = \dfrac{L\sqrt{m^*}}{\hbar\pi\sqrt{2}}\displaystyle\sum_{n,m}\int_0^{\infty}\delta\left[x + (E_x)_n + \left(E_y\right)_m - E\right]\frac{1}{\sqrt{x}}dx \end{cases} \tag{15.41}$$

Using Eq. (5.43) and the same argument as Eq. (15.), we obtain:

$$g_{1D}(E) = \frac{L}{\pi\hbar}\sqrt{\frac{m^*}{2}}\sum_{m,n}\frac{\Theta\left(E - \left[(E_x)_n + \left(E_y\right)_m\right]\right)}{\sqrt{E - \left[(E_x)_n + \left(E_y\right)_m\right]}} \tag{15.42}$$

This expression means that, in a quantum wire, the density of states depends on the energy like $1/\sqrt{E}$ in each of the subband defined by two consecutive energy levels $(E_x)_n + (E_y)_m$, as shown in Fig. 15.8.

Equation (15.42) also reveals infinite divergences at points where the energy E coincides with the bottoms of quasi-one-dimensional subbands at $(E_x)_n + (E_y)_m$.

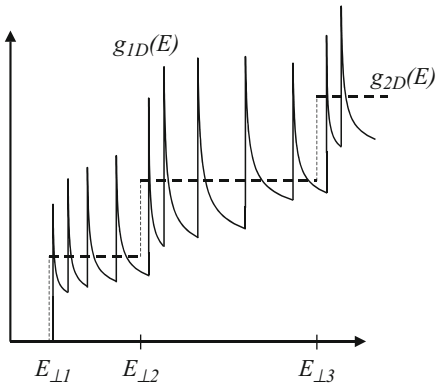

Fig. 15.8 Density of states in the conduction band for a quantum wire (1D). For comparison, the density of states of a quantum well (2D) is shown in dashed lines

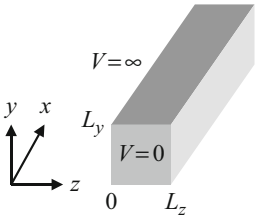

Fig. 15.9 The infinitely deep rectangular cross-sectional quantum wire

These discontinuities take place in an idealized model. In real structures, they are smeared out by the electron collisions mentioned earlier, in Sect. 15.6.1. The maximum values of g_{1D} in Fig. 15.8 are not infinite but correspond to the value of Eq. (15.42) when the denominator is equal to $E - [(E_x)_n + (E_y)_m] \approx \hbar/\tau$, where τ is the electron lifetime discussed earlier.

15.7.2 Infinitely Deep Rectangular Wires

The simplest quantum-wire geometry would have a rectangular cross section surrounded by infinite barriers. This is illustrated schematically in Fig. 15.9 and can be considered to be the two-dimensional analogy to the one-dimensional confinement potential of the standard infinitely deep quantum well.

Within the quantum wires, the potential is zero, while outside the wire, it is infinite. Thus the wavefunction outside the quantum wire should be zero. The form of the potential is $V(y, z) = V(y) + V(z)$, and it is separable. Hence the Schrödinger equation within the wires for the motion along the two directions of confinement (y and z) is:

$$-\frac{\hbar^2}{2m^*}\left[\frac{\partial^2\Psi(y,z)}{\partial y^2}+\frac{\partial^2\Psi(y,z)}{\partial z^2}\right]=E_{y,z}\Psi(y,z) \tag{15.43}$$

The separation of the coordinates in the Schrödinger equation allows the motion to be decoupled further and leads to:

$$\Psi(y,z)=\Psi(y)\Psi(z), \tag{15.44}$$

and then the Schrödinger equation can be written as:

$$-\frac{\hbar^2}{2m^*}\Psi(z)\frac{\partial^2\Psi(y)}{\partial y^2}-\frac{\hbar^2}{2m^*}\Psi(y)\frac{\partial^2\Psi(z)}{\partial z^2}=\left(E_y+E_z\right)\Psi(y)\Psi(z) \tag{15.45}$$

Here the energy components can also be separated into $E_{y,\,z}=E_y+E_z$.
The decoupling is completed with the following equations:

$$-\frac{\hbar^2}{2m^*}\frac{\partial^2\Psi(y)}{\partial y^2}=E_y\Psi(y) \tag{15.46}$$

$$-\frac{\hbar^2}{2m^*}\frac{\partial^2\Psi(z)}{\partial z^2}=E_z\Psi(z) \tag{15.47}$$

The above equations are exactly the same as the infinite quantum well problems (see Sect. 4.4.3, Eq. (4.44) and Eq. (4.45)). The wavefunction solutions are:

$$\Psi(y)=\sqrt{\frac{2}{L_y}}\sin\left(\frac{\pi n_y y}{L_y}\right) \tag{15.48}$$

and

$$\Psi(z)=\sqrt{\frac{2}{L_z}}\sin\left(\frac{\pi n_z z}{L_z}\right) \tag{15.49}$$

which give the components of the energy as:

$$E_y=\frac{\hbar^2\pi^2 n_y^2}{2m^*L_y^2} \tag{15.50}$$

$$E_z=\frac{\hbar^2\pi^2 n_z^2}{2m^*L_z^2} \tag{15.51}$$

Thus, the total energy of the particle due to the confinement is given by the sum of the two discrete components:

$$E_{y,z} = \frac{\hbar^2 \pi^2}{2m^*}\left(\frac{n_y^2}{L_y^2} + \frac{n_z^2}{L_z^2}\right) \tag{15.52}$$

The confined states of a quantum wire are described by the two principal quantum numbers n_y and n_z, and this is in contrast to the single number required for the one-dimensional case discussed in Chap. 4.

15.8 Zero-Dimensional Structures: Quantum Dots

15.8.1 Density of States

An ideal quantum dot, also known as a quantum box, is a structure capable of confining electrons in all three dimensions, thus allowing zero dimension (0D) in their degrees of freedom. In quantum dots, there is thus no possibility for free particle-like motion. The energy spectrum is completely discrete, similar to that in an atom, as will be briefly derived below.

In a quantum dot of rectangular shape, the wavefunction of an electron does not involve any plane wave component, in contrast to other low-dimensional quantum structures. The total energy is the sum of three discrete components:

$$\begin{aligned} E(n,m,l) &= (E_x)_n + \left(E_y\right)_m + (E_z)_l \\ &= \frac{\hbar^2 (k_x)_n^2}{2m^*} + \frac{\hbar^2 \left(k_y\right)_m^2}{2m^*} + \frac{\hbar^2 (k_z)_l^2}{2m^*} \end{aligned} \tag{15.53}$$

where n, m, and l are integers (1,2,...) used to index the quantized energy levels, $(E_x)_n$, $(E_y)_m$, $(E_z)_l$, and quantized wavenumbers, $(k_x)_n$, $(k_y)_m$, and $(k_z)_l$, which result from the confinement of the electron motion in the x-, y-, and z-directions, respectively. The values for $(E_x)_n$, $(E_y)_m$, and $(E_z)_l$ can be determined, for example, by solving the finite potential well problem in Sect. 4.4.4 in all three directions.

As for the quantum wire, the most important characteristic of a quantum dot is its electron density of states in the conduction band which is given by:

$$\begin{aligned} g_{0D}(E) &= 2\sum_{n,m,l} \delta[E(n,m,l) - E] \\ &= 2\sum_{n,m,l} \delta\left[(E_x)_n + \left(E_y\right)_m + (E_z)_l - E\right] \end{aligned} \tag{15.54}$$

There is no further simplification of this expression. The density of states of zero-dimensional electrons consists of Dirac functions, occurring at the discrete energy levels $E(n,m,l)$, as shown in Fig. 15.10.

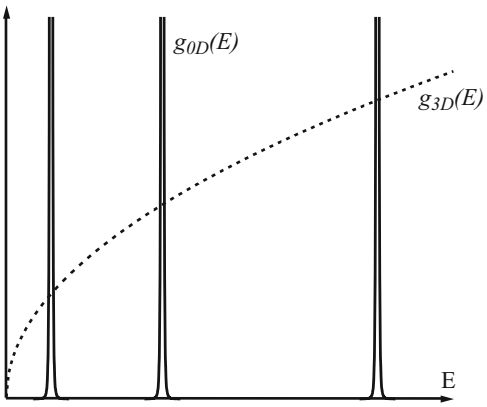

Fig. 15.10 Density of states in the conduction band for a quantum dot (0D). For comparison, the density of states of a bulk crystal (3D) is shown

Again, the divergences in the density of states shown in Fig. 15.10 are for ideal electrons in a quantum dot and are smeared out in reality by a finite electron lifetime τ.

Since quantum dots have a discrete, atom-like energy spectrum, they can be visualized and described as "artificial atoms." This discreteness is expected to render the carrier dynamics very different from that in higher-dimensional structures where the density of states is continuous over a range of values of energy. For example, since all energy states are not allowed, changes in the electron configurations are more restricted.

15.8.2 Infinite Spherical Quantum Dot

The similarity between quantum dots and isolated atoms is close when considering the case of spherical quantum dots, i.e., when the confining potential has a spherical symmetry. For example, nanocrystals in semiconductor-doped glasses and colloidal solutions often have a spherical shape. When the passivation of the surface is made in such a way that carriers are strongly confined in the nanocrystal, the system is usually correctly described by an infinitely deep spherical well, where the confining potential is zero inside and infinite outside a spherical quantum dot with the radius R. The potential can therefore be expressed as:

$$\begin{cases} V\left(\vec{r}\right) = 0 & \text{if } r < R \\ V\left(\vec{r}\right) = \infty & \text{otherwise} \end{cases} \tag{15.55}$$

Due to the spherical symmetry of the potential, the Schrödinger-like equation for the envelope function $\Psi\left(\vec{r}\right)$ in spherical coordinates is given as:

Table 15.2 Values of α_{nl} for the lowest states in a spherical well

n,l	Level	α_{nl}
10	1S	3.142
11	1P	4.493
12	1D	5.763
20	2S	6.283
13	1F	6.988
21	2P	7.725

$$\left[-\frac{\hbar^2}{2m^*}\left(\frac{1}{r^2}\frac{\partial}{\partial r}\left(r^2\frac{\partial}{\partial r}\right)-\frac{\vec{L}^2}{r^2}\right)+V(\vec{r})\right]\Psi(\vec{r})=E\Psi(\vec{r}) \tag{15.56}$$

where $\vec{L}^2$ is the orbital momentum operator which commutes with the Hamiltonian. The solution to Eq. (15.56) is the extension of the one-dimensional problem to the three-dimensional one. The eigenstates are products of the spherical harmonics Y_{lm} and of radial parts given below. The energies and wavefunctions of an infinite spherical quantum dot are:

$$\begin{aligned} E_{nl} &= \frac{\hbar^2}{2m^*}\left(\frac{\alpha_{nl}}{R}\right)^2, \quad n=1,2,3\ldots, \quad l=0,1,2\ldots \\ \Psi(r,\theta,\varphi) &= Aj_l\left(\frac{\alpha_{\mathrm{nl}}r}{R}\right)Y_{lm}(\theta,\varphi) \end{aligned} \tag{15.57}$$

where A is a constant, j_l is a spherical Bessel function, n is the positive integer, and l is the angular momentum quantum number. The coefficients α_{nl} are the zeros of the spherical Bessel functions labeled by an integer in order of increasing energy. Some values of α_{nl} are given in Table 15.2 for the lowest levels defined by n and l. The levels can be labeled with the usual atomic notation, e.g., 1s corresponds to $l=0$ and $n=1$. Their degeneracy is however not the same as in real atoms, and there is no restriction on the values of l for a given n like in free atoms where $l<n$. This is due to the different nature of the potential which in this case encapsulates the particle and its orbit. The degeneracy is only in terms of the allowed "m" values which range from $+l$ to $-l$.

15.9 Optical Properties of Low-Dimensional Structures

Figure 15.11 illustrates the band diagram in a GaAs-AlGaAs quantum well with several electron and hole subbands and the notations used in this section.

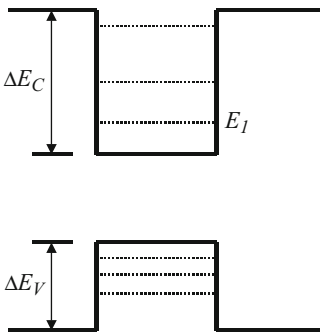

Fig. 15.11 Schematic of band diagram of GaAs-AlGaAs quantum well with electron and hole subbands

15.9.1 Interband Absorption Coefficients of Quantum Wells

The absorption coefficient for a transition from a valence band state of energy E_1 to a conduction band state of energy E_1 has been given earlier in Chap. 10 and can be written as:

$$\alpha(\hbar\omega) = \frac{\pi q^2}{cm_0^2 \bar{n}\varepsilon_0 \omega V} \sum_{1,2} |p_{12}|^2 (f_1 - f_2)\delta(E_{12} - \hbar\omega) \tag{15.58}$$

where:

$$p_{12} = \left\langle 1 \middle| \exp\left(-i\vec{k}_{\lambda} \cdot \vec{r}\right) \vec{e}_{\lambda} \cdot \vec{p} \middle| 2 \right\rangle \tag{15.59}$$

and $\bar{n}$ is refractive index of the medium and V is the volume. f_1 and f_2 are the Fermi occupational probabilities for electrons in the respective states. We assume the incoming photon with the wavevector $\vec{k}_{\lambda}$ and the polarization vector $\vec{e}_{\lambda}$. In the present situation, an electron in the mth heavy-hole subband with 2D wavevector $\vec{k}_{\mathrm{h}}$ absorbs a photon and enters a state with wavevector $\vec{k}_{\mathrm{e}}$ in the nth subband of the conduction band. In terms of the 2D vector $\vec{\rho}$ and the coordinate z normal to the quantum-well layer plane, the wavefunctions are then written as:

$$\begin{aligned} |1\rangle &= \left| h, m, \vec{k}_h \right\rangle = U_h(\vec{\rho}, z) \exp\left(i\vec{k}_h \cdot \vec{\rho}\right) \phi_{hm}(z), \\ |2\rangle &= \left| c, n, \vec{k}_e \right\rangle = U_c(\vec{\rho}, z) \exp\left(i\vec{k}_e \cdot \vec{\rho}\right) \phi_{cn}(z), \end{aligned} \tag{15.60}$$

where U_h and U_c are the cell-periodic parts of the Bloch function and ϕ's are envelope functions. We decompose the photon wavevector as $\vec{k}_\lambda = \left(\vec{k}_{\lambda//}, k_{\lambda z}\right)$ and write Eq. (15.29) as:

$$p_{12} = \left| \left\langle c, n, \vec{k}_e \middle| \exp\left(i\vec{k}_{\lambda//} \cdot \vec{\rho} + ik_{\lambda z} z\right) \vec{e}_\lambda \cdot \vec{p} \middle| h, m, \vec{k}_h \right\rangle \right| \tag{15.61}$$

The matrix element can be evaluated by using Eq. (15.60) for the wavefunctions and integrating over ρ and z. The photon wavevector is considered negligible in comparison to the carrier wavevectors. Thus electron momentum is conserved for the in-plane motion only. However, since the motion is quantized along z-direction, there is no such selection rule for this direction. Using the k-conservation rule and the relation $\vec{k}_\mathrm{e} = \vec{k}_\mathrm{h} + \vec{k}_{\lambda//} \approx \vec{k}_\mathrm{h}$, the squared matrix element can be written as:

$$|p_{12}|^2 = \left\langle |p_{cv}|^2 \right\rangle_{QW} \delta_{\vec{k}_e, \vec{k}_h} C_{mn} \tag{15.62}$$

with

$$C_\mathrm{mn} = |\langle \phi_\mathrm{hm} | \phi_{cn} \rangle|^2 = \left| \int \phi^*_\mathrm{hm} \phi_\mathrm{cn} dz \right|^2 \tag{15.63}$$

In the present case, $\langle |p_{cv}|^2 \rangle_{QW}$ is the polarization-dependent momentum matrix element for transitions between conduction and valence subbands in a quantum well. It is different from the momentum matrix element in bulk semiconductors. The factor $\langle \phi_\mathrm{hm} | \phi_\mathrm{cn} \rangle$ denotes the overlap between the electron and the hole envelope wavefunctions. For infinite potential barriers with parabolic band model, both ϕ_hm and ϕ_cn are sinusoidal functions, and the overlap integral becomes zero unless n is equal to m. Thus in this ideal situation, the optical selection rule is expressed as $C_\mathrm{mn} = \delta_\mathrm{mn}$. However, in real situation the finiteness of the barriers ΔE_c and ΔE_v and also the change in the effective masses of the barriers cause a deviation from the above perfect selection rule.

We can write for the absorption coefficient:

$$\alpha(\hbar\omega) = \frac{\pi q^2}{c m_0^2 \bar{n} \varepsilon_0 \omega V} C_{mn} \sum_{\vec{k}_\mathrm{e}, \vec{k}_\mathrm{h}} \left\langle |p_{cv}|^2 \right\rangle_{QW} \delta_{\vec{k}_\mathrm{e}, \vec{k}_\mathrm{h}} (f_\mathrm{e} - f_\mathrm{h}) \delta\left(E_\mathrm{e}\left(\vec{k}_\mathrm{e}\right) - E_\mathrm{h}\left(\vec{k}_\mathrm{h}\right) - \hbar\omega \right) \tag{15.64}$$

Using the parabolic $E\left(\vec{k}\right)$ relation, the energies are expressed as:

$$\begin{cases} E_{\mathrm{e}}\left(\vec{k}_{\mathrm{e}}\right) = E_{\mathrm{cn}} + \dfrac{\hbar^2 k_{\mathrm{e}}^2}{2m_e} \\ E_{\mathrm{h}}\left(\vec{k}_{\mathrm{h}}\right) = -E_{\mathrm{g}} - E_{\mathrm{hm}} - \dfrac{\hbar^2 k_{\mathrm{h}}^2}{2m_{\mathrm{h}}} \end{cases} \tag{15.65}$$

The Fermi occupational probability can be written as:

$$f(E) = \frac{1}{1 + \exp\left[\left(E - E_f\right)/k_{\mathrm{b}}T\right]} \tag{15.66}$$

where E_{f} is the quasi-Fermi level. Using $\vec{k}$-conservation, the double summation in Eq. (15.64) is reduced to a single summation over $\vec{k}_{\mathrm{h}}$. The argument of the energy-conserving δ-function then becomes:

$$E_{\mathrm{e}}\left(\vec{k}_{\mathrm{e}}\right) - E_{\mathrm{h}}\left(\vec{k}_{\mathrm{h}}\right) - \hbar\omega = \left(E_{\mathrm{g}} + E_{\mathrm{cn}} + E_{\mathrm{hm}}\right) - \frac{\hbar^2 k_{\mathrm{h}}^2}{2m_r} - \hbar\omega, \tag{15.67}$$

where m_r is the reduced mass (Eq. 10.80). The remaining sum in Eq. (15.64) becomes:

$$\sum_{\vec{k}_{\mathrm{h}}} \rightarrow \frac{2S}{(2\pi)^2} \int \delta\left(E_{\mathrm{g}} + E_{\mathrm{cn}} + E_{\mathrm{hm}} - \frac{\hbar^2 k_{\mathrm{h}}^2}{2m_{\mathrm{r}}} - \hbar\omega\right) 2\pi k_{\mathrm{h}} dk_{\mathrm{h}} \left[f_{\mathrm{h}}(k_{\mathrm{h}}) - f_{\mathrm{e}}(k_{\mathrm{h}})\right] \tag{15.68}$$

where S is the area of the quantum well and factor 2 is from spin degeneracy. The integration in Eq. (15.68) is performed easily due to the presence of the δ-function, so that we obtain:

$$\alpha(\hbar\omega) = \frac{m_r q^2 C_{\mathrm{mn}} \left\langle |p_{cv}|^2 \right\rangle_{QW}}{\varepsilon_0 \hbar^2 c m_0^2 \bar{n} \omega L} \left(f_{\mathrm{e}} - f_{\mathrm{h}}\right) H\left(\hbar\omega - E_{\mathrm{g}} - E_{\mathrm{cn}} - E_{\mathrm{hm}}\right) \tag{15.69}$$

where L is the thickness of the quantum well and $H(x)$ is the Heaviside step function. Equation (15.69) may be compared with the expression for bulk. Remember from Chap. 5 that $|p_{vc}|^2$ can be expressed and estimated in terms of the Kane matrix elements (Eq. (5.67) and Sect. 5.7). In both cases, the absorption coefficients are proportional to the respective joint density of states function. The expected variation of absorption coefficients are shown in Fig. 15.12. The experimental measurements of absorption coefficient in GaAs/AlGaAs quantum wells and thick GaAs layer are compared in Fig. 15.12.

When considering intersubband absorption, we immediately have the selection rule that normal incident light with (x,y) polarization cannot be absorbed because the z-confined wavefunctions are orthogonal. In order for light to be absorbed in an intersubband transition, it is essential that there should also be a z-polarized component giving an qzE_z coupling term.

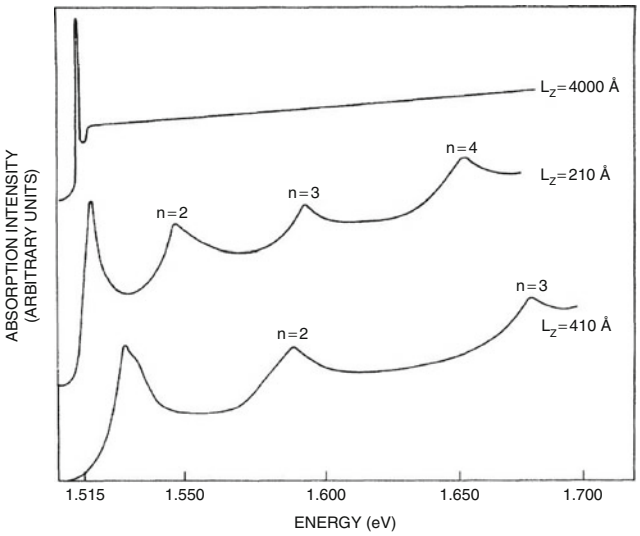

Fig. 15.12 Absorption coefficient in GaAs/AlGaAs quantum wells and thick GaAs layers (upper curve). The peaks correspond to quantum-confined subband n (Reprinted figure with permission from Dingle R, Wiegmann W, and Henry CH, Phys Rev Lett (Vol. 33): p. 829, Fig. 2. Copyright 1974 by the American Physical Society)

15.9.2 Absorption Coefficient of Quantum Wires

The calculation of the absorption coefficient may be performed as usual by assuming the $\vec{k}$-conservation condition to be valid along the direction of the free motion. The absorption coefficient is written as:

$$\alpha(\hbar\omega) = -B_1 \sum_{\vec{k}} (f_e - f_h)\delta\left(E_g + \hbar^2 k^2/2m_r - \hbar\omega\right) \tag{15.70}$$

where B_1 is a constant and E_g denotes the effective gap which is bulk bandgap plus the electron and hole subband energies. The summation over $\vec{k}$ may be converted into an integral, and assuming $f_e - f_h = 1$ the integration may be performed to yield:

$$\alpha(\hbar\omega, a) = -\frac{q^2 C_{1D}\left\langle |p_{cv}|^2 \right\rangle_{QWR} (2m_r)^{1/2}}{2m_0^2 \varepsilon_0 \bar{n}\omega c S} \left(\hbar\omega - E_g\right)^{-1/2} \tag{15.71}$$

where the coefficient C_{1D} is the overlap integral of a quantum wire and $\langle |p_{cv}|^2 \rangle_{QWR}$is the momentum matrix element for transitions between conduction and valence subbands in a quantum wire. S is the cross-sectional area of the wire.

Equation (15.71) leads to the conclusion as noted before that the absorption coefficient is proportional to the joint density of states function. Therefore the absorption coefficient should show a singularity at $\hbar\omega = E_g$ and fall with increasing photon energy as shown in Fig. 15.8.

15.9.3 Absorption Coefficient of Quantum Dots

The absorption coefficient of a cubic QD system of side length a may be written as:

$$\alpha(\hbar\omega) = \frac{2\pi q^2 \left\langle |p_{cv}|^2 \right\rangle}{m_0^2 \bar{n} \varepsilon_0 c \omega a^3} \sum_m g(m^2) \delta\left(\hbar\omega - E_g - \frac{\pi^2 \hbar^2 m^2}{2 m_r a^2}\right) \tag{15.72}$$

where $g(m^2)$ is the degeneracy of the energy level determined by m^2. Only $\Delta m = 0$ transitions are allowed. Equation (15.72) indicates that the interband absorption in a QD will be a series of discrete lines, representing the reduced density of states function of a 0D system. The discrete lines will occur at photon energies:

$$\hbar\omega = E_g + \frac{\pi^2 \hbar^2 m^2}{2 m_r a^2} \tag{15.73}$$

In practice the absorption spectra are not discrete lines but are broadened because of the size distribution of quantum dots. We consider that the family of dots has a fluctuation in side length described by the following Gaussian distribution:

$$P(a) = \frac{1}{(2\pi)^{1/2} D} \exp\left[-\frac{(a - a_0)^2}{2D^2}\right] \tag{15.74}$$

where a_0 is the average value and $D^2 = \langle (a - a_0)^2 \rangle$ is the standard deviation.

Using Eq. (15.72) and Eq. (15.74), the absorption coefficient for a nonuniform quantum dot system can be calculated as:

$$\alpha = \int_0^\infty P(a) \alpha(\hbar\omega, a) da \tag{15.75}$$

The line broadening also occurs due to phonon scattering processes in addition to the size distribution of QDs.

15.10 Examples of Low-Dimensional Structures

The optical properties of low-dimensional quantum structures, arising from their peculiar density of states, are often put to use in semiconductor optoelectronic devices, such as semiconductor laser diodes and quantum-dot infrared photodetectors. Such low-dimensional structures are fabricated in practice using a succession of processes involving epitaxy, lithography, and etching. An illustration of the principle of quantum wells, wires, and dots is shown in Fig. 15.13.

Low-dimensional quantum structures have, for example, been most beneficial for semiconductor laser diodes, leading to low threshold current (minimum necessary current for lasing), high power, and weak temperature-dependent devices. These

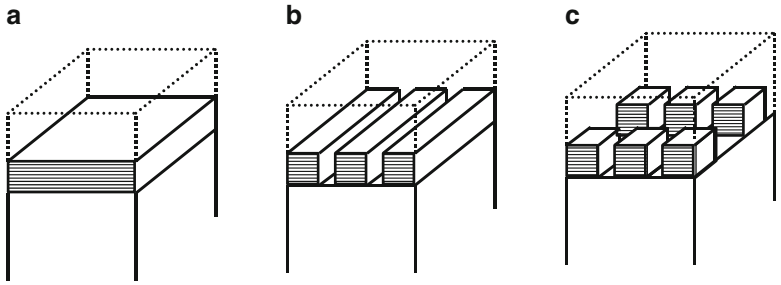

Fig. 15.13 Illustration of a (**a**) 2D structure (quantum well), (**b**) 1D structure (quantum wires), and (**c**) 0D structure (quantum dots), showing the various levels of spatial confinement

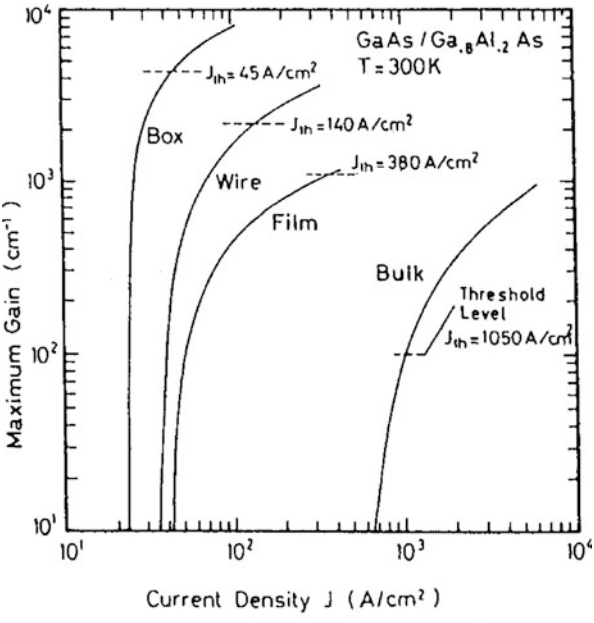

Fig. 15.14 Coefficient of light amplification (gain) for different structures. The dashed lines show the threshold current density above which laser emission starts (Reprinted with permission from IEEE Journal of Quantum Electronics Vol. 22, Asada M, Miyamoto Y, and Suematsu Y, "Gain and the threshold of 3-dimensional quantum-box lasers," p. 1918, Fig. 6. Copyright 1986, IEEE)

properties, in conjunction with their small size, have made laser diodes attractive for applications involving densely packed laser arrays. This applies also to the monolithic integration of lasers with low-power electronics such as computer optical interconnects, optoelectronic signal processing, and optical computing.

An illustration of the effect of low-dimensional quantum structures on the properties of optoelectronic devices is shown in Fig. 15.14 which illustrates the theoretical predictions for threshold currents in semiconductor lasers based on active regions with different low-dimensional structures. By using quantum dots instead of a bulk layer, the threshold current may be reduced by more than 20 times. This is due to the abrupt energy dependence of the density of states in low-dimensional quantum structures which can enhance the light amplification mechanisms and thus allows lasing to occur at lower currents.

15.10.1 Quantum Wires

Figure 15.15 shows an example of a quantum wire, which has been etched in a thin film of doped GaAs deposited on an undoped GaAs substrate. Inside the rectangular stripe, there is a highly conductive channel where the electrons are confined and which forms a quantum wire and whose width is narrower than that of the stripe. In GaAs wires, the minimum diameter of the channels can be about 80 nm.

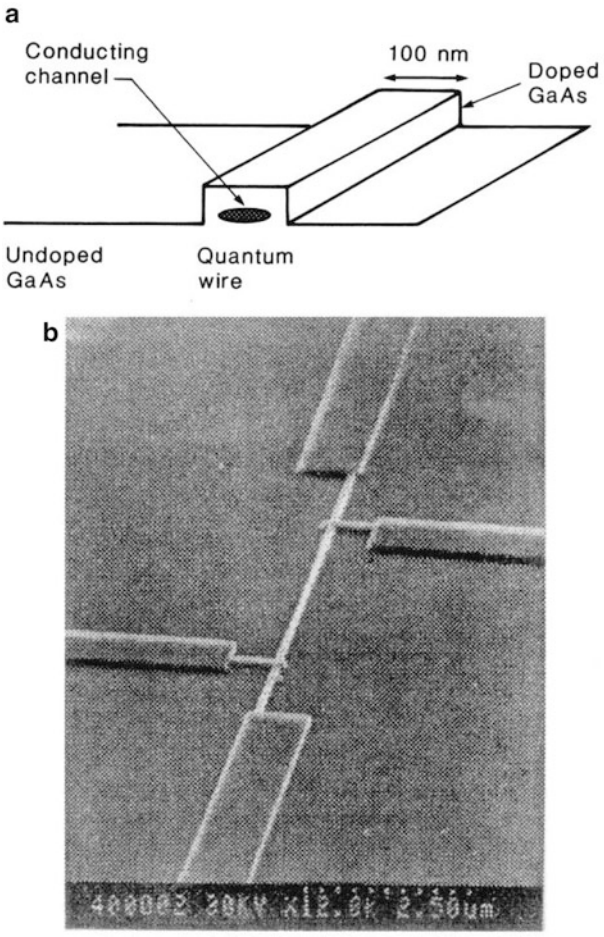

Fig. 15.15 Quantum wire formed by etching away all but a thin strip of doped semiconductor on an undoped substrate: (**a**) schematic diagram; (**b**) practical example ("Fig. 11.1", from Low-Dimensional Semiconductors: Materials, Physics, Technology, and Devices by M.J. Kelly; taken after Physica Scripta Vol. T45, Beaumont SP, "Quantum wires and dots: defect related effects," p. 196. Copyright 1992, Physica Scripta. Reprinted with permission of Oxford University Press, Inc. and The Royal Swedish Academy of Sciences)

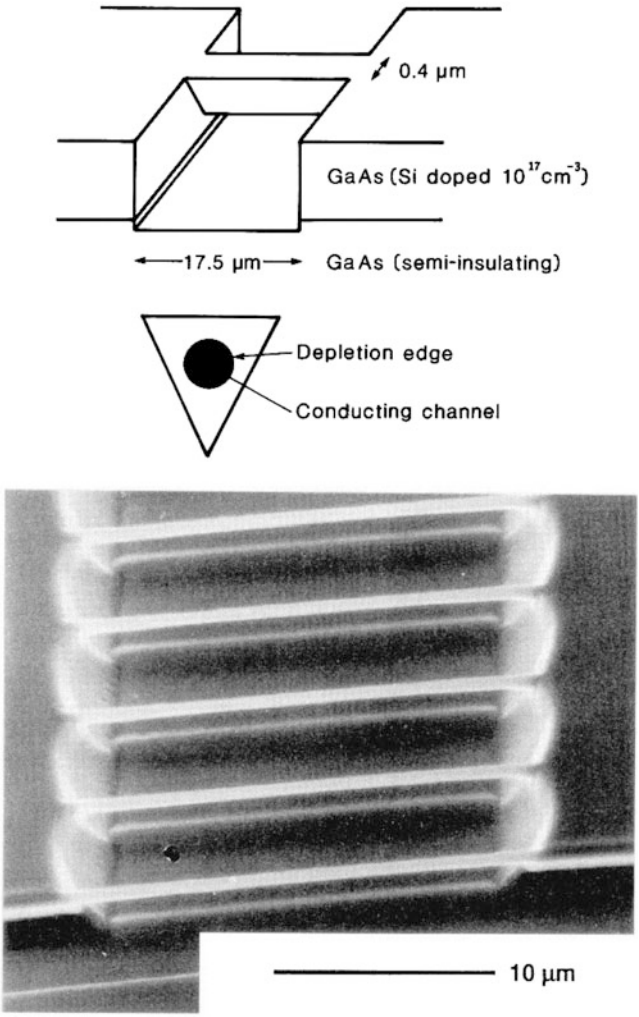

Fig. 15.16 Schematic diagram and image of quantum wires of doped GaAs on an insulating substrate (Taken from Fig. 11.2 of "Low-Dimensional Semiconductors: Materials, Physics, Technology, and Devices" by MJ Kelly; taken after Journal of Vacuum Science and Technology B Vol. 6, Hasko DG, Potts A, Cleaver J.R.A., Smith CG, and Ahmed H, "Fabrication of submicrometer freestanding single-crystal gallium arsenide and silicon structures for quantum transport studies," p. 1851. Copyright 1988, American Institute of Physics. Also taken after Physica Scripta Vol. T54 Kelly, et al." Quasi-One-Dimensional Transport in Semiconductor Microstructures" p.201, Fig. 1 (a), Copyright 1992 Royal Swedish Academy. Reprinted with permission of Oxford University Press, Inc., American Institute of Physics)

Another example of quantum wire is shown in Fig. 15.16. The structure was made by using etching a doped thin GaAs film, in such a way that it undercuts the crystal from the surface, i.e., GaAs material is removed *below* the remaining stripe.

The resulting structure thus has a triangular cross section, and a highly conductive channel is present inside it which is where the electrons are confined and a quantum wire is formed.

Quantum wires have novel optical absorption spectra which depend on the polarization of the light. The optical properties can be computed with the methods we discussed in Chap. 10. Again the key quantity and novelty will be mainly due to the joint density of states. But more recently, scientists have discussed another reason why the quantum wire may be of interest, and this is in the context of electron-electron interactions having a stronger effect on carrier mobility. The dense many-electron quantum wire is also called the Luttinger liquid (Bockrath et al. 1999) and exhibits an exciting new science which has been studied only very recently. When moving along a "line," carriers are more likely to be affected by each other's Coulomb interaction. A carrier will find it difficult or even impossible in some cases to pass another charge or to avoid the other charge, if for some reason this charge is blocked on the way. One trapped carrier in the wire can stop the entire flow of current, which is an example of the Coulomb blockade. The controlled blockage and removal of the blockage is one of the targets of present-day nanotechnology research. In this way, the presence or absence of a single charge in a trap can give rise to a measurable quantity of electrical current. The quantum wire is especially interesting if all the electron spins are pointing in one direction. This can be done either because they have been aligned by a magnetic field or because they have been injected into the wire by a magnet. Quantum wires can therefore be used as "spin wires" which transport spin information from one area of a device to the other.

The fabrication of quantum pillars or vertical quantum wires, as shown in Fig. 15.7, in doped (multilayer) semiconductors is more complicated. The processing steps are shown in Fig. 15.17c and d which result in the structure shown in Fig. 15.17b. A submicrometer-diameter metal dot is laid down onto the film (step 2 in Fig. 15.17c), and the pillar structures are formed by an etching process (step 3), through which parts of the material are selectively removed. The electrons are thus confined laterally inside the pillars (4). This structure is then filled with polyimide, a polymeric material, and etched back to expose the top of the metal dot (steps 1 and 2 in Fig. 15.17d). The whole surface can then be coated with metal (steps 3 and 4), making contact to the metal dots and thus the vertical quantum wire. The fabrication methods can be refined so that any single pillar can be contacted.

15.10.2 Quantum Dots

The structures shown in Fig. 15.17 can also be used as a quantum dot if the carriers can be confined vertically at the top and bottom of the pillars, in addition to being confined laterally by the side walls of the pillars. This can be achieved by choosing the two barrier layers (AlGaAs in Fig. 15.17a) that are sufficiently thick.

Another method of realizing semiconductor quantum dots consists of making use of a strain-induced transformation that occurs naturally in the initial stages of growth of lattice-mismatched materials. This type of growth usually starts atomic layer by

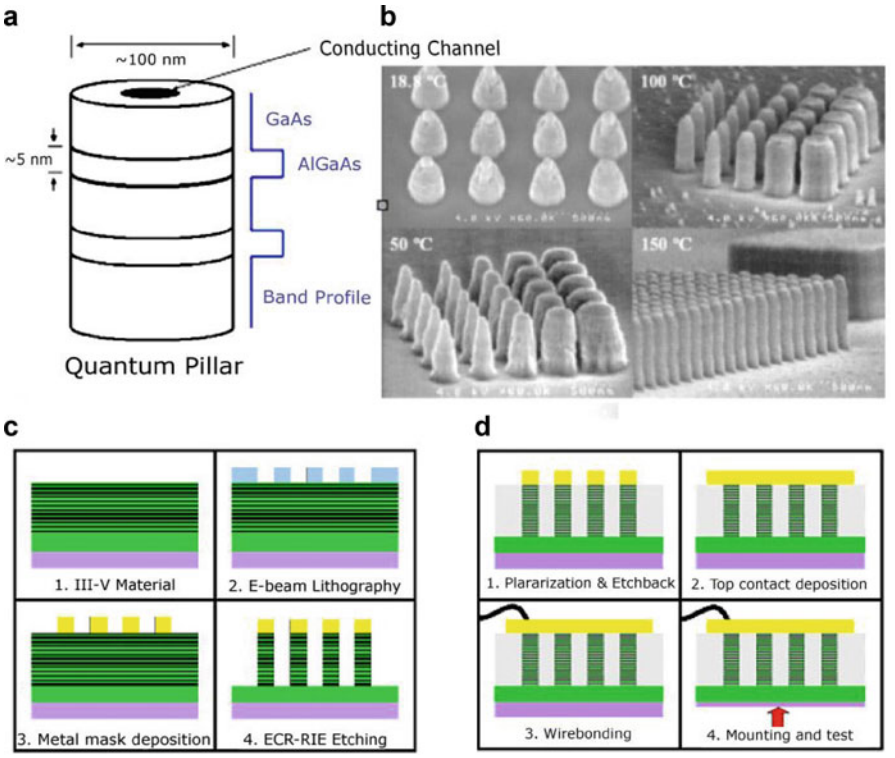

Fig. 15.17 A quantum pillar formed from resonant tunneling semiconductor multilayers showing (**a**) a schematic diagram of the pillar, (**b**) the partially processed structure after the first etch, and (**c**) and (**d**) the full processing route

atomic layer, and after a certain critical thickness is reached, nanometer-size islands spontaneously form. This is known as the Stranski-Krastanov growth mode. These islands show good size uniformity and large surface densities. In this method, the growth has to be interrupted immediately after the island formation and before the islands reach a size for which strain relaxation and defects occur. This spontaneous island formation during growth precludes the interface quality problems often associated with low-dimensional quantum structures achieved through etching. This breakthrough has created some excitement in the physics community by providing the opportunity for experimental verification of the effects of three-dimensional quantum confinement in semiconductor structures.

Several reports worldwide show remarkable agreement on the optical properties of these structures, finding that the delta function density of states expected from 0D quantum structures manifested itself in ultrasharp light emission peaks. Compound semiconductors that have been used until now for quantum dots include InAs and InGaAs on GaAs, InAlAs on AlGaAs, InAs on InP, and InP on InGaP and GaP.

15.10.3 Effect of Electric and Magnetic Fields

In the confined direction of the quantum well or in nanopillars and quantum dots, the electrons subjected to an electric field cannot wonder away to infinity, so the electric field constitutes a relatively small perturbation and can be handled by methods of quantum-mechanical perturbation theory. The same is true for nanopillars and quantum dots in a magnetic field. The expansion of energy levels and wavefunctions can be usually stopped in second order, giving us a powerful way of estimating field-induced changes in energies and optical permittivities. In Chap.10, we showed how permittivity can be related to the wavefunctions and energy spectrum (Eq. 10.53)). In static fields, we can work with the time-independent Schrödinger equation and perturbation theory. Following Sect. 4.3.1, we can calculate the new ground-state wavefunction to first-order and energy to second-order perturbation theory using Eq. (4.205) and Eq. (4.207). The perturbation caused by an electric field E_{0z}applied in the z-direction is $-qzE_{0z}$ giving the second order (first order vanishes by symmetry in a symmetric coordinate system):

$$E_{\mathrm{g}}^{(2)} = \sum_{l} (aE_{0z})^2 \frac{\left|z_{gl}\right|^2}{E_g - E_l} \tag{15.76}$$

In a confined system, the electric field-induced shift of the energy of the free subband eigenstates is called the Stark shift and is lowering of energy when we start with box eigenstates. Figure 15.18 shows the absorption spectra of a quantum well in

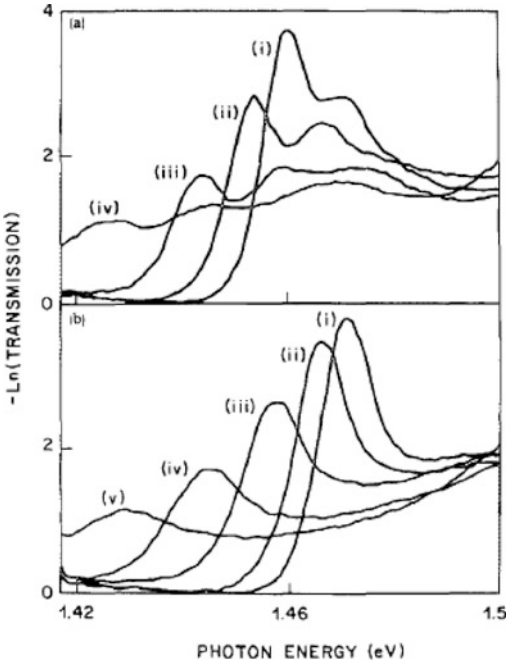

Fig. 15.18 Electro-absorption spectra of GaAs quantum-well waveguide device as a function of electric field applied field perpendicular to the plane of the layers. (i) = 1.6×10^4 V·cm^{-1}; (ii) = 10^5V·cm^{-1}; (iii) = 1.4×10^5V·cm^{-1}; (iv) = 1.8×10^5V·cm^{-1}; (v) = 2.2×10^5V·cm^{-1} (Reprinted with permission from Applied Physics Letters Vol. 47, Weiner JS, Miller D. A.B., Chemla DJ, Damen TC, Burrus CA, Wood T H, Gossard AC, Wiegmann W, "Strong polarization sensitive electro-absorption in GaAs/AlGaAs quantum well waveguides," p. 1149. Copyright 1985, American Institute of Physics)

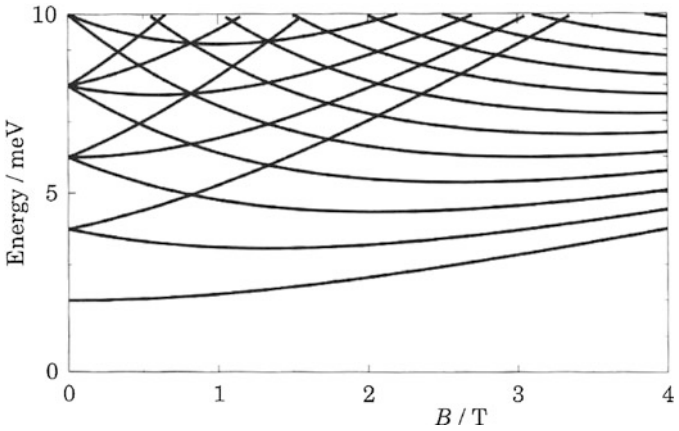

Fig. 15.19 The energy levels of a parabolically confined quantum dot with intrinsic energy level splitting $\hbar\omega_0 = 2$meV in a magnetic field (Davies JH, The Physics of Low Dimensional Semiconductors: an Introduction, p. 237, Fig. 6.16. © Cambridge University Press 1998. Reprinted with the permission of Cambridge University Press)

an electric field applied perpendicular to the layers and also shows the Stark energy shift of the exciton peak. The action of an electric field on an exciton can however in some cases be more complex than just a Stark shift, especially when the exciton is broken up by the field, and then the simple method might not suffice.

Figure 15.18 shows the effect of a magnetic field on the energy levels of a large quantum dot in which electrons are confined by a three-dimensional parabolic potential, with energy levels at ~2 meV interval (Fig. 15.19).

In this example the magnetic energy levels and the intrinsic confinement level splittings are comparable at $B = 1$ T, so the effect of the B field is obviously large. In smaller dots, one needs a correspondingly larger B field to see the same relative shifts or a smaller effective mass. When the magnetic coupling is treated in perturbation, both the first-order and the second-order terms contribute to the energy. In the notation of Chap. 10 and from Eq. (10.113), the perturbation is of the form (m^* is the effective mass):

$$V = \left[(qBx)^2 - 2qBx\left(i\hbar\frac{\partial}{\partial y}\right)\right]\frac{1}{2m^*} \tag{15.77}$$

The first-order perturbation shift in energy is positive, and the second-order term is necessarily negative. The B field will in general raise the energy of the electron when it is in the ground state.

Finally Fig. 15.20 shows the drastic effect a magnetic field has on the longitudinal and Hall resistance of a high-quality, high-mobility quantum well. The magnetic field is applied perpendicular to the plane in which conduction takes place. We explained in Chap. 10 how the magnetic field produces Landau levels and how the degeneracy of the levels changed with B and that the Fermi energy in Landau levels

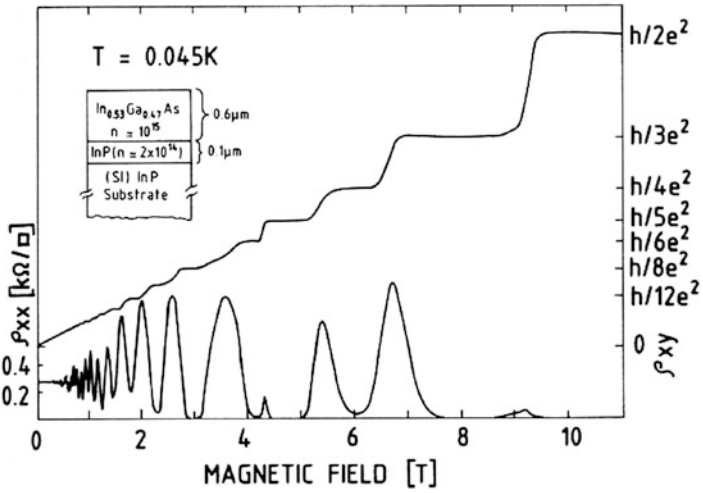

Fig. 15.20 Shubnikov-de Haas trace (ρ_{xx}) and quantum Hall effect (ρ_{xy}) as a function of magnetic field normal to the plane at $T = 0.045$ K in $Ga_{0.47}In_{0.53}As$-InP heterostructures (Reprinted with permission from Applied Physics Letters Vol. 48, Razeghi M, Duchemin JP, Portal JC, Dmowski L, Remeni G, Nicolas RJ, and Briggs A, "First observation of the Quantum Hall effect in a $Ga_{0.47}In_{0.53}As$-InP heterostructure with three electric subbands," p. 712. Copyright 1986, American Institute of Physics)

moves with B field for a given electron concentration. Increasing the magnetic field increases the Landau level splittings and the degeneracy of each band. This then implies that the density of states at the Fermi level changes too. The Fermi level can move from a region of finite to a region of zero density of states, i.e., sit in the gap between two adjacent Landau levels. But this then according to Eq. (10.39) drastically changes the longitudinal resistance with B field exactly as shown in Fig. 15.20. In contrast to the longitudinal resistance, we see that the Hall resistance does not vanish when the Fermi level is in the Landau gaps but forms plateaus until the Fermi level again crosses into the middle of the next Landau band, at which point the resistance suddenly goes up again with B field. This fascinating phenomenon is known as the quantum hall effect or QHE. The plateau signifies that in this interval of level filling (B decreasing) or emptying (B increasing), the number of Hall carriers is not changing. We see a plateau in the gap and not zero conductance because the Hall voltage is not a Fermi level property. When the Fermi level crosses a region of small density of states, i.e., from the maxima through the gaps, then it is passing through energy levels which are spatially localized; the orbits of the localized states form closed paths which do not intersect the sample edge. The energy levels which are affected by the B field are the delocalized ones which sit in a narrow region in the maxima and obey $\varepsilon_n = (n + 1/2)\hbar\omega_c$. Remember that in the semiclassical description, the Hall voltage exists because the Lorentz force creates an asymmetric charge redistribution for drifting carriers.

15.11 Summary

In this chapter, we have first reviewed topics associated with semiconductor heterostructures. In particular, the concepts of type I and type II band alignments were outlined. Furthermore, model solid theory and Anderson's model for heterojunction energy band alignment and diagram were described.

Subsequently, we showed that the motion of electrons in a crystal can be spatially confined in one, two, or even three directions, by designing and fabricating an adequate semiconductor structure, a quantum well, wire, or dot. When the amount of confinement is sufficient, quantum-mechanical effects become important and lead to the discretization of the energy spectrum, i.e., the quantization of allowed energy levels becomes an important feature of the system. A rough criterion is as always $\Delta E_{n,\ n\ +\ 1} \sim k_{\mathrm{b}}T$, i.e., the splitting has to be bigger or comparable to the thermal energy.

The important new characteristic of a low-dimensional quantum structure is the new density of states. This quantity shows a different dependence on energy, especially for lower (wire and dot) dimensionality systems. The magnitude and energy dependence of the density of states strongly correlates with many properties of the solid and in particular with the optical properties of a semiconductor. This has been shown here and in Chap. 10. We have shown how electric and magnetic fields affect confined eigenstates and eigenenergies. Ironically it is often easier to estimate the effect of external fields in confined systems than in infinite ones because energy levels are discrete and wavefunctions normalized in a small volume. This means that one can use standard second-order perturbation theory. Confinement can be exploited in the design of the characteristics of optoelectronic devices. Having evaluated changes to energies and wavefunctions, it is possible to compute the electro-optic coefficients using the methods of Chap. 10 combined with the perturbation expansion given here.

Problems

1. In this chapter, we used the effective mass of the electron in the Schrödinger equation. Explain why it was necessary to do so, whereas it was not necessary in the infinite and finite potential well in Chap. 4.
2. Give an expression (an integral) for the total number of electrons in the conduction band of a bulk three-dimensional semiconductor and then in the first subband of a quantum well of width L in terms of the density of states and the Fermi function (assume box eigenstates in the confined direction). If at $T = 0$ K we dope the first subband in the conduction band and we fill all the states in the first subband, how many electrons do we need per unit area?
3. Consider a 50 Å GaAs and 300 Å $Al_{0.6}Ga_{0.4}As$ layers forming a quantum well structure.

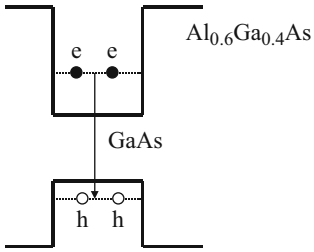

The electrons are all located at the first energy state (e), and holes are at (h). The general expression of the first energy state is determined as $E_1 = \hbar^2\pi^2/2m^*a^2$, where a is the width of the quantum well and m^* is the effective mass of the particle considered (for holes, consider the heavy-hole effective mass).

What is the photon energy of the light emitted when the electron and the hole recombine as shown in the above figure?

4. Let us assume a quantum dot which is spherical. The electrons or holes are confined at energy states with the following expression: $E_{nl} = (\hbar^2/2m^*)(\alpha_{\mathrm{nl}}/R)^2$, where m^* is the effective mass of the electron or hole and the value of α_{nl} is given by $\alpha_{10} = \pi$, $\alpha_{11} = 4.49$, $\alpha_{12} = 5.76$, $\alpha_{20} = 6.28$, $\alpha_{21} = 7.72$, and $\alpha_{22} = 9.09$. Now consider the very small GaAs quantum dots of radius 10 nm. If the electron drops from the second state (α_{11}) to the first state (α_{10}), what is the photon energy of the light emitted from this transition?

   Draw the energy diagram for GaAs quantum dots with radius 5 nm, 10 nm, and 15 nm. How does the first energy state change as a function of radius?

5. *Density of States of an Ideal Two-Dimensional Electron Gas*

   Using the infinite barrier approximation, derive an expression for the density of states for electrons in a quantum well in terms of the well width L and electron effective mass m^*.

6. *Fermi* Energy *of an Ideal Two-Dimensional Electron Gas*

   Consider a structure consisting of two GaAs quantum wells that have been grown far apart in $Al_xGa_{1-x}As$ with the same Al composition x ($x \leq 0.3$). In well A the GaAs thickness is L, while in well B, it is $2L$. Now, approximate the conduction bands in wells A and B by ideal quantum wells between infinitely high potential barriers. Suppose that the quantum wells contain electrons and that both wells have the same Fermi energy,$E_F = 3F_1^A$ where E_1^A is the lowest quantized energy level in well A.

   (a) How many subbands in each well contain electrons at zero temperature?
   (b) What is the two-dimensional charge density N_A and N_B in each well? Give the answer in terms of known physical quantities such as $\hbar$ and L.

7. *The* Graphic *of the Two-Dimensional Density of States*
   Figure 15 shows the density of states of a quantum well. The confinement energy of the lowest level (E_1) is 17 meV, and the first excited state (E_2) has a confinement energy of 30 meV. The Fermi level is located 50 meV above the bottom of the conduction band. Determine the number of electrons contained in the well.
8. The two-dimensional potential which confines the electrons in a quantum wire made of GaAs is assumed to be parabolic, and the subband separation is given as $\hbar\omega_0 = 12$ meV. If the Fermi energy is $E_F = 37$ meV as measured from the bottom of the lowest subband, calculate the number of electron per unit length at 0 K including spin degeneracy.
9. *The* Moss-*Burstein Shift in Absorption Spectra*
   The "band filling" or Moss-Burstein shift effect occurs in all heavily doped three-dimensional semiconductors. It is a consequence of the fact that electrons are fermions, and therefore it is impossible (by the Pauli exclusion principle) to optically excite an electron into a same spin k-state, which is already occupied. In the case of strongly degenerate n^+-doped sample, this has the effect of prohibiting any interband transition into electron states below the Fermi energy leading to an upward shift in the effective absorption edge, E'_g (see figure below). The *Moss-Burstein shift* (ΔE) is defined as the difference between the effective absorption edge and the energy gap (E_g) of the material, i.e., $\Delta E = E'_g - E_g$.

   (a) Calculate the *Burstein shift* in the absorption edge of a direct semiconductor with parabolic bands due to the heavy doping (n-type) at very low temperature ($T \approx 0$ K). The carrier concentration is n_e. Neglect excitons. Note that the shift is not simply the Fermi energy of the electrons and involves the mass of both conduction and valence bands.
   (b) Calculate the *Moss-Burstein shift* for the GaAs material doped with 1×10^{18} electrons/cm^3. What should happen to the shape of the absorption edge? Assume $m_e^* = 0.067\, m_0$ and $m_h^* = 0.45\, m_0$ where $m_0$is the electron rest mass.

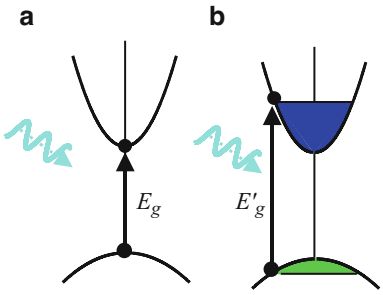

Allowed optical transitions in direct-gap semiconductors: (**a**) undoped material, absorption threshold of E_g; (**b**) n^+-doped material, absorption threshold blue shifted to E_g' by the Moss-Burstein shift

10. *Critical Radius of a Spherical Quantum Dot with Finite Barrier Height*
Assume that a quantum dot has a spherical shape with radius R and is surrounded by a medium of higher bandgap such as AlGaAs. The potential barrier at the conduction band is ΔE_c at all points in the surface of the sphere. The potential well is a square well of height, ΔE_c, for $r > R$ and is 0 for $r < R$. Let us consider the simplest case of zero angular momentum ($l = 0$), and then it follows that the wavefunctions $\Psi(\vec{r})$ depends only on the radial part. When $l = 0$ and $\Psi(\vec{r}) = R(r) = \phi(r)/r$, Eq. (15.56) reduces to:

$$\begin{cases} -\dfrac{\hbar^2}{2m^*}\dfrac{d^2\phi(r)}{dr^2} + \Delta E_c\phi(r) = E\phi(r) & (r > R) \\ -\dfrac{\hbar^2}{2m^*}\dfrac{d^2\phi(r)}{dr^2} = E\phi(r) & (r < R) \end{cases}$$

The solution of the above equation is the same as the one with a one-dimensional finite potential well. Find the critical radius below which there is no bound state of one electron in the quantum dot.

References

Bockrath M, Cobden DH, Lu J, Rinzler AG, Smalley RE, Balents L, McEuen PL (1999) Luttinger liquid behaviour in carbon nanotubes. Lett Nat 397:598–601
Shockley W (1951) U.S. Patent 2,569,347

Further Reading

Ahmed H (1986) An integration microfabrication system for low dimensional structures and devices. In: Kelly MJ, Weisbuch C (eds) The physics and fabrication of microstructures and microdevices. Springer, Berlin, pp 435–442
Ashcroft NW, Mermin ND (1976) Solid state physics. Holt, Rinehart, Winston, New York
Bassani F, Pastori Parravicini G (1975) Electronic states and optical transitions in solids, Chap. 6. Pergamon, New York
Bastard G (1988) Wave mechanics applied to semiconductor Heterostructures. Halsted Press, New York
Beaumont SP (1992) Quantum wires and dots-defect related effects. Phys Scr T45:196–199
Chuang SL (1995) Physics of optoelectronic devices. John Wiley & Sons, Inc., New York
Davies JH (1998) The physics of low dimensional semiconductors: an introduction. Cambridge University Press, New York
Dingle R Confined carrier quantum states in ultrathin semiconductor heterostructures. In: Queisser HJ (ed) Feskorperproblem XV, pp 21–48
Einspruch NG, Frensley WR (1994) Heterostructures and quantum devices. Academic Press, London

Hasko DG, Potts A, Cleaver JR, Smith C, Ahmed H (1988) Fabrication of sub-micrometer free standing single crystal GaAs and Si structures for quantum transport studies. *J Vac Sci Technol B* 6:1849–1851

Rosencher E, Vinter B (2002) Optoelectronics. Cambridge University Press, Cambridge

Scherer A, Jewell J, Lee YH, Harbison J, Florez LT (1989) Fabrication of microlasers and microresonator optical switches. Appl Phys Lett 55:2724–2726

Sze S (1981) Physics of semiconductor devices, 2nd edn. John Wiley & Sons, Inc., New York

Tewordt M, Law V, Kelly M, Newbury R, Pepper M, Peacock C (1990) Direct experimental determination of the tunneling time and transmission probability of electrons through a resonant tunneling system. J Phys Condens Matter 2:896–899

Vasko FT, Kuznetsov AV (1999) Electronic states and optical transitions in semiconductor heterostructures. Springer, New York

Weisbuch C, Vinter B (1991) Quantum semiconductor structures. Academic Press, New York